Journal of the European Ceramic Society 22 (2002) 2595–2602

www.elsevier.com/locate/jeurceramsoc

Microstructure of Y_2O_3 doped Al_2O_3–ZrO_2 eutectics grown by the laser floating zone method

J.I. Peña, R.I. Merino, N.R. Harlan[1], A. Larrea, G.F. de la Fuente, V.M. Orera*

Instituto de Ciencia de Materiales de Aragón, C.S.I.C., Universidad de Zaragoza, 50009 Zaragoza, Spain

Received 30 October 2001; received in revised form 20 February 2002; accepted 7 March 2002

Abstract

Al_2O_3–ZrO_2 eutectics containing 9 mol% Y_2O_3 (with respect to zirconia) were produced by directional solidification using the laser floating zone (LFZ) method. The eutectic microstructures were investigated as a function of the growth variables. Using a solidification-axis thermal gradient of 600 °C/mm a homogeneous, colony-free, interpenetrating lamellar microstructure was obtained for growth rates less than 50 mm/h. Higher growth rates produce cellular structures. Colonies grew with the [0001] alumina and the [110] zirconia axis parallel to the growth direction. The uniform lamellar microstructure obtained at low growth rates is stable during thermal treatment at 1500 °C.

Keywords: Al_2O_3; Composites; Eutectics; $ZrO_2(Y_2O_3)$

1. Introduction

Micro-composite material systems can be fabricated via the solidification of eutectic melts. These composites are highly homogeneous, present strongly bonded phases as well as a high density of interfacial area together with short interphase distances. The combination of these properties produces an improvement of the material properties, particularly excellent mechanical behavior and thermal stability up to near the melting temperature.[1,2]

Al_2O_3–ZrO_2 melt-grown eutectics are surprisingly tough at room temperature and up to near the eutectic point.[3] As they are very resistant to grain growth and creep, they are candidates for applications where a combination of high strength and toughness at high temperature and chemical inertness are needed. In a previous work the relationship between the mechanical properties and the microstructure in these compounds was studied.[4] The microstructure was a very decisive aspect in determining the mechanical properties of the sample. In fact, the colony was the critical defect in these samples. The microstructure resulting from different solidification procedures using either the Bridgman,[5] floating zone melting,[6,7] edge-defined film-fed growth,[8] or micro-pulling down methods,[9] has been studied previously. Recently, the production of large plates of Al_2O_3–ZrO_2 eutectic composites by laser zone melting has been reported.[10] However, because of the difficulty in controlling and reproducing experimental conditions the relationship between processing parameters and microstructure is still uncertain.

When solidified directionally they usually show a columnar colony microstructure; colonies are formed by faceted alumina grains grown along the [0001] sapphire c-axis which contain a very fine and regular dispersion of ZrO_2 rods. The grains are surrounded by a coarse granular microstructure.[11] The colony size decreases as the growth rate increases,[12] and it is replaced by a lamellar microstructure near the rod edge in rod shaped samples.[3,11] Understanding this transition is very important in order to improve the material properties. Unfortunately, the situation is far from being clear. For example, Courtright et al.[7] reported that the microstructure changed from fibrous to lamellar as the growth rate increased. However, Echigoya et al.[6] and Lee et al.[9] found that the degenerated lamellar microstructure was obtained for slow growing rates.

* Corresponding author. Tel.: +34-976-761-333; fax: +34-976-761-229.

E-mail address: orera@posta.unizar.es (V.M. Orera).

[1] Ford foundation Post-Doctoral Fellow, USA, present address: CETENASA, Noain, Navarra, Spain.

0955-2219/02/$ - see front matter
PII: S0955-2219(02)00121-8

In this work, rods of Al_2O_3–ZrO_2(9 mol% Y_2O_3) were grown using the laser floating zone (LFZ) method. The principal goal was to search for growth parameters to achieve a homogeneous, colony-free microstructure that is expected to provide better mechanical properties than the colony structure owing to the smaller size of the defects.[4,13] The orientation relationship between the component phases and the thermal stability as a function of the different microstructures were also studied.

2. Experimental procedure

Starting materials were commercially available Al_2O_3 (99.99%, Aldrich), ZrO_2 (99+%, Alfa) and Y_2O_3 (99.99%, Aldrich) powders. The powders were milled in a vibratory micro-mill (model MM2000, Retsch, Haan, Germany) with alumina components, fired in air at 1000 °C for 1 h, hand-milled in an agate mortar and mixed into the desired compositions. The composition of the samples was 62 mol% Al_2O_3–34.5 mol% ZrO_2–3.5 mol% Y_2O_3. It was formulated along the liquidus line between the eutectic point of the binary Al_2O_3–ZrO_2 system and the peritectic of the ternary Al_2O_3–ZrO_2–Y_2O_3 system as given by Lakiza and Lopato.[14] Precursor rods were prepared by isostatically pressing the powder for 2 min at 200 MPa. The compacts were fired for 12 h at 1250 and 1500 °C to increase density and handling strength. The laser floating zone (LFZ) method[15] and a CO_2 laser were used to directionally solidify the eutectic rods at a variable growth rate between 10 and 1500 mm/h. The effect of the rotation of either the precursor ceramic rod or the melt-grown eutectic rod or both was studied for rotation speed between 0 and 200 rpm (revolutions per minute). The diameter of the grown rod was varied from 1.8 mm to near 1 mm. The ratio between the diameters of the melt-grown rod and precursor were kept around 0.7. The length of the molten zone was of the order of the rod diameter.

Thermal gradients along the growth axis were measured using a near infrared (0.9–1.2 μm) radiometer with a spatial resolution of about 0.5 mm. The eutectic liquid strongly absorbs the visible light which is in contrast with the relatively high transparency of the molten Al_2O_3.[16] Consequently, the measured temperature reflects the temperature of the sample surface rather than that of the bulk. The unknown emissivity was estimated to be $e \approx 0.9$ by adjusting the measured temperature in the gas–melt–solid interface to the melting point of the eutectic ($T_m = 1860$ °C). Since the liquid–solid interface can not be directly visualized the shape of this interface was studied in longitudinal sections of samples quenched from melt by abruptly switching off the laser power.

Transverse and longitudinal cross-sections of the grown rods were cut and polished for optical microscopy, scanning electron microscopy (SEM), and X-ray diffraction analysis. The microstructure was studied using a SEM (model 6400, Jeol, Tokyo, Japan). The statistics to obtain the colony size was typically performed over 15 colonies. For the smaller rods and lamellae it was done over one hundred features. X-ray diffraction was performed using a D-max Rigaku system with a rotating anode. (CuK_α radiation, step size = 0.03° 2θ, count time = 1 or 5 s).

3. Results and discussion

Determination of the component phases was carried out using both Raman spectroscopy and X-ray diffraction (XRD) techniques. The eutectic samples are composed of α-alumina and cubic zirconia phases.

3.1. Processing parameters and microstructure

In the LFZ technique the thermal gradients at the liquid–solid interface are very steep. In this case, melt solidification is almost a self-quenching process which allows rapid growth rates and highly concentrated impurities. However, steep temperature gradients also result in excessive thermal stress which may produce cracking and other defects. Crystal growth takes place along the thermal gradient. Consequently, flat and stable liquid–solid interfaces favor the formation of stable growth fronts. Another point of concern is the heating source, in this case, the CO_2 laser radiation. Since the absorption coefficient of the molten oxides of the laser radiation is high,[10] the laser radiation is absorbed in a region within about 0.1 mm of the laser exposed external surface. Heating of the internal regions of the sample takes place via thermal diffusion. Capillary convection also takes place in the melt and may seriously perturb the flatness of the liquid-solid interface. Thus, the size of the melt and hence of the crystal diameter, is limited in this case to a few cubic millimeters and less than 2 mm, respectively.

Thermal gradient is the most important growth parameter. To achieve a homogeneous microstructure, coupled eutectic growth is necessary. Coupled growth is possible when constitutional supercooling is avoided, that is, when the axial thermal gradient complies with the inequality[17]

$$(dT/dz) > v\Delta T/D \quad (1)$$

where v is the growth rate, ΔT the localized supercooling due to concentration gradients and D the chemical diffusion constant. High thermal gradients are then required. However, in the cylindrical geometry used, axial gradients always induce radial thermal gradients which may produce cracking. A compromise

exists between the need for large thermal gradients to avoid the effects of constitutional supercooling and the maximum acceptable gradient to avoid cracking.

In the LFZ technique the thermal gradient is controlled by thermal diffusion to the external atmosphere and along the rod, growth rates, crystal diameter, etc.[18] Brice proposed the following expression for the temperature distribution in a growing rod,[19]

$$T(r,z) = T_m + (T_m - T_0)\frac{(1 - hr^2/2R)}{1 - hR/2}\exp\left[-(2h/R)^{1/2}z\right] \quad (2)$$

where h is the cooling constant, T_0 the ambient temperature, T_m the melting temperature and R the radius of the rod. The origin of coordinates is taken at the rotation axis in the liquid–solid interface. The measured temperature profile closely follows Eq. (2). By fitting this equation to the experimental temperature profile leaving T_0 and h as fitting parameters we obtained typical values of 300 °C and 0.5 cm^{-1}, respectively. The axial and radial thermal gradients can be easily calculated from Eq. (2). Since $hR << 1$ for the small rod diameters grown, at the interface $z=0$ these gradients are:

$$(dT/dz)_{z=0} \approx (2h/R)^{1/2}(T_m - T_0) \quad (3)$$

which is essentially independent of the distance to the rotation axis and

$$(dT/dr)_{z=0} \approx r(h/2R)^{1/2}(dT/dz) \quad (4)$$

which is linearly dependent on r. Using the measured thermal profile we calculate the gradient at the solidification interface which is 6×10^5 °C/m. According to the Brice model, to grow an uncracked crystal the axial thermal gradient must be

$$(dT/dz) < 4\varepsilon/\alpha h^{1/2}R^{3/2} \quad (5)$$

where α is the thermal expansion coefficient and ε the breaking strain. The breaking strain in the eutectic is unknown but it is expected to be larger than those of the component phases, i.e., 2.0×10^{-4} for $ZrO_2(Y_2O_3)$ crystal and 2.8×10^{-4} for sapphire.[20] Using Eq. (5), we calculated the maximum axial thermal gradient for zirconia and sapphire single crystals as a function of the rod diameter. The results are given in Table 1. It can be seen that the size of the rods that can be grown with the thermal gradient we are using is limited to radii less than 0.5 mm for zirconia and 1 mm for sapphire. In the case of the eutectics, and especially for the low growth rate samples, we find experimentally that to ensure long rods free of cracks it is necessary to grow samples with $R<0.8$ mm.

The characteristic size of the microstructure features showed a tendency to decrease from center to edge.

Table 1
Maximum axial thermal gradients (in K/cm units) for different crystal radii (in cm)

Crystal radius	0.05	0.1	0.2
ZrO_2–Y_2O_3[a]	8×10^3	2.7×10^3	1.0×10^3
Sapphire[a]	2.5×10^4	8.8×10^3	3×10^3

[a] Parameters taken from Ref. 21.

Rotation helps to homogenize temperatures and also to decrease capillary convection. With a 200 rpm precursor rotation, flat liquid-solid interfaces and hence homogeneous microstructures along the rod transverse cross sections were obtained. It is worth noting that even for the relatively low value of the thermal diffusivity ($a=9.5\times10^{-7}$ m^2 s^{-1} [21]) the Péclet number, defined as $P_e=Rv/a$, was smaller than unity even for the highest used growth rate (1500 mm/h). Consequently, the axial thermal gradient is not expected to vary significantly with growth speed.

The most important remaining processing parameter that can be varied is the growth rate. In Fig. 1 the microstructures observed in the transverse sections of eutectic rods grown at different growth rates are shown. At the lowest growth rate, $v=10$ mm/h, a homogeneous, coupled eutectic microstructure defined by two three-dimensional interpenetrating networks is obtained. The homogeneous microstructure that extends throughout the rod cross section consists of irregular ZrO_2 lamellae (light phase) in a continuous Al_2O_3 matrix (dark phase). The thickness of the ZrO_2 lamellae ranges from 1 to 2 μm. No amorphous phase or primary phase grains were detected.

Increasing the growth rate dendrites start to develop and the solidification suffers a transition from the planar to the cellular regime. At 300 mm/h faceted cells consisting of a Al_2O_3 matrix with a triangular dispersion of embedded, orderly zirconia fibers of about 0.3 μm diameter is observed. The colonies are surrounded by a coarser structure. An alumina-yttria-rich phase (gray color) is identified in this inter-colony region. A similar observation has been reported before, where was assigned to the yttrium aluminum garnet phase.[3] In Table 2 the microstructural properties obtained from the analysis of the SEM images are summarized. The size of the colonies is maximum at $v\approx150$ mm/h and decreases for higher growth rates. At the highest achieved growth rates the colony structure is almost completely substituted by a nearly homogeneous cell structure with lamellae on it which resembles the structure obtained at low growth rates. This is a characteristic behavior of eutectic growth when one of the phases has a high entropy of fusion. Likely, the system follows the laws of competitive growth, which explains the development of dendrites or cells in the solidified eutectic for intermediate growing rates. According to that

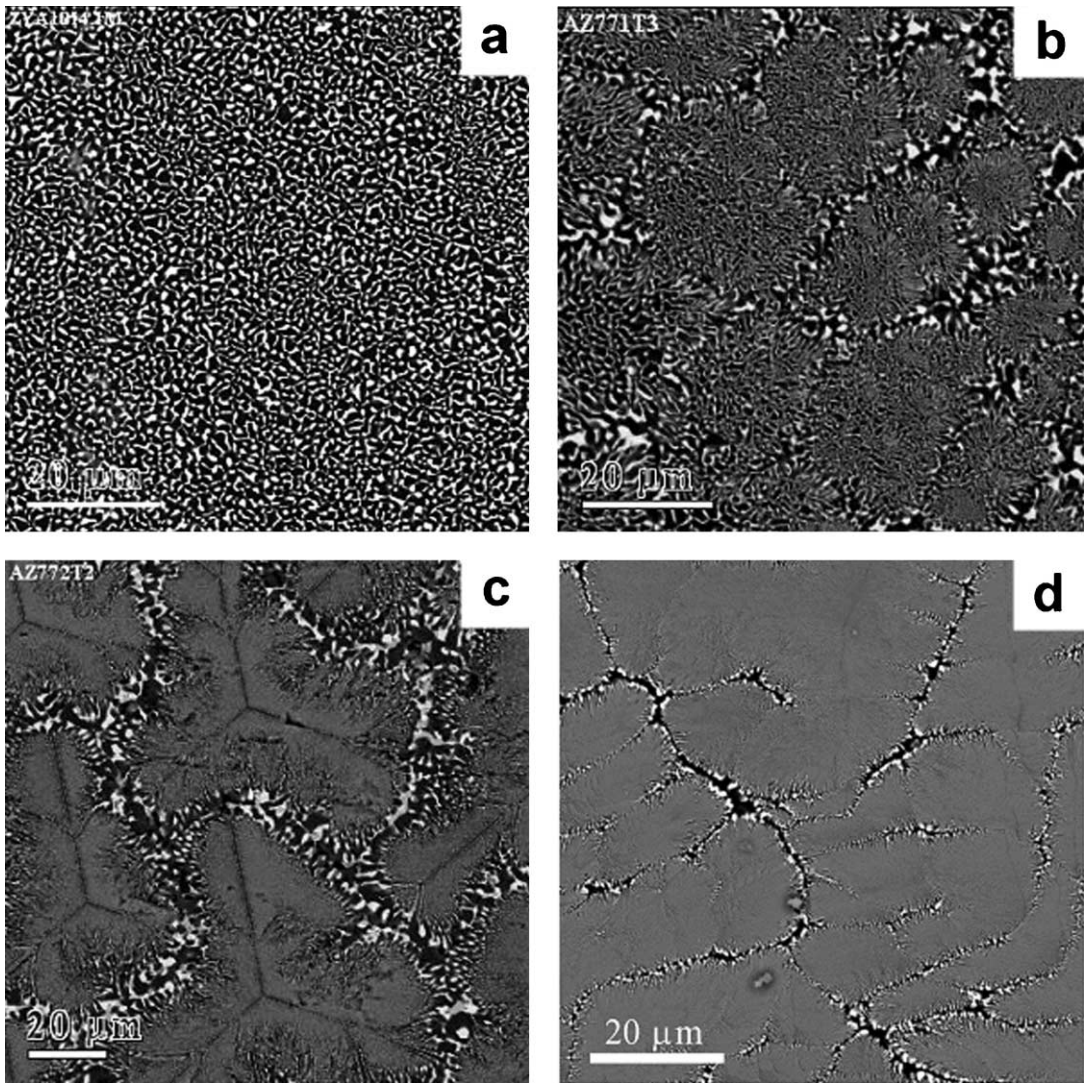

Fig. 1. SEM micrographs of transverse sections of Al_2O_3–$ZrO_2(Y_2O_3)$ eutectics grown at (a) 10 (b) 100 (c) 300 and (d) 1500 mm/h. Bright phase is c-ZrO_2 and dark phase α-Al_2O_3. Scale bars = 20 μm.

Table 2
Microstructure features size (in μm) as a function of the growth rate (in mm/h). Data were taken from the center of the rod

Growth rate	1500	300	200	150	100	75	50	20	10
Colonies	20	70	95	100	20	20	[e]	[e]	Coupled
ZrO_2[a]		2	3	2.5	5	3.5	4	3	1.5 c
ZrO_2[b]	0.08[c]	0.3[d]	0.3[d]	0.3[d,c]	[c]	[c]	[c]	[c]	

[a] Intercolony.
[b] Intracolony.
[c] Lamella.
[d] Fibers.
[e] Transition from cellular to coupled.

model homogeneous eutectic microstructures should form at both low and high growth velocities.[22]

The transition from the coupled to the cellular regime takes place in this system at rates of about 50 mm/h. Using the thermal diffusion coefficient given by Bourban et al.[21] in Eq. (1), a supercooling of about 15 K is calculated. It was also observed that coupled growth was possible at higher growth rates for thinner samples. As stated by Eq. (3) decreasing the rod radius induces an increase in the axial thermal gradient and the inequality given by Eq. (1) will be fulfilled for higher growth rates.

3.2. Crystallography

The crystal growth directions and relative phase orientations were determined using the preferential orientation effects observed in XRD patterns on selected rod planes using both theta and alpha-scans. XRD patterns obtained from the transverse sections of eutectic samples grown at the different rates between 10 to 300 mm/h are shown in the Fig. 2. The XRD patterns are formed basically by the {111} and {220} zirconia reflections at 30.1 and 50.2°, respectively, and {0006} at 41.7° and {0001$\underline{2}$} at 90.8° for alumina. At first glance these results are compatible with a preferential orientation of the alumina phase with the c-axis parallel to the growth direction and two zirconia variants, the majority growing along the [110] axis and some, less frequently, along the [111] axis. To discuss these details we will focus on the two extreme cases of samples grown at 300 and 10 mm/h.

Eutectics grown at high growth rates present a microstructure of regularly distributed trigonal elongated cells similar to that recently reported by Lee et al.[9] In Fig. 3 the XRD patterns obtained on the transverse and longitudinal cross sections of an eutectic sample grown at 300 mm/h are given, with the microstructures shown in Fig. 1c. The longitudinal section has been done, as sketched in Fig. 4. The colonies consist of Al_2O_3 single crystals, 70 μm diameter and 1 mm length, with ZrO_2 fibers of about 0.3 μm diameter. Optical microscopy shows that one of the three ZrO_2 rod sets are parallel to the longitudinal section plane and at an angle of approximately 60° from the colony axis (i.e. the growth axis), whereas the other two sets follow the trigonal symmetry shown in the transverse cross-section.

The preferential orientation observed in the XRD diagrams allow the determination of the orientation of the phases in both cross-sections. These orientations are depicted in Fig. 4. It is worth noting that in the longitudinal $(1\bar{2}10)$ plane the alumina *R*-axis can be found at 57.6° from the *c*-axis. Since the zirconia fibers grow parallel to this *R* direction, a growth model for the eutectics with the colony structure can be tentatively proposed. In this model, the alumina which has the largest entropy of fusion is the phase which plays the leading role during solidification. In the uncoupled growth regime, the alumina crystals grow along the *c*-axis but with *R*-plane facets. In fact, rhomboid facets have been found when Al_2O_3 single crystals grew along the [0001] direction.[23] In the eutectic, the ZrO_2 fibers will grow perpendicular to these planes and parallel to the alumina *R* direction. This growth process would cause the conspicuous triangular shape observed in the transverse sections. The crystallographic orientation reported in Fig. 4 is the dominant one. Some of the Al_2O_3 grains have a different orientation, which is the one that results from rotating the above given Al_2O_3

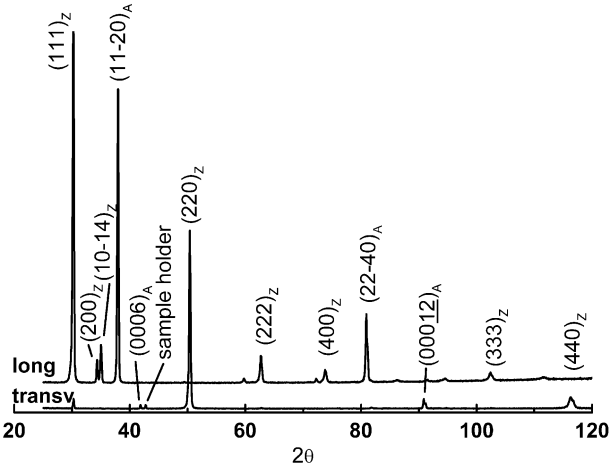

Fig. 3. XRD patterns measured in transverse and longitudinal sections of an Al_2O_3–$ZrO_2(Y_2O_3)$ sample grown at 300 mm/h.

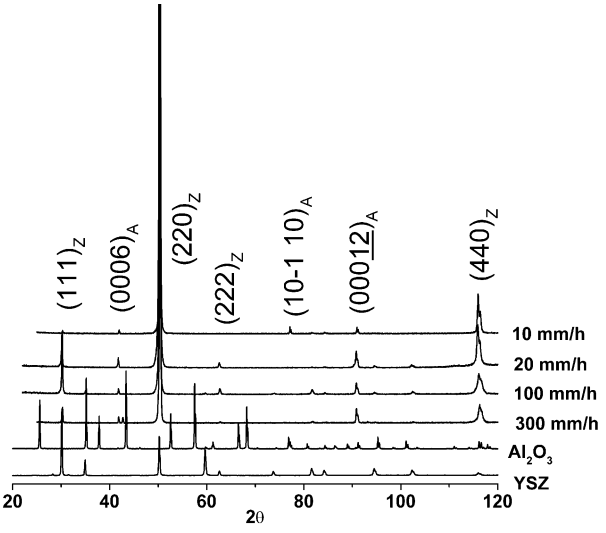

Fig. 2. XRD patterns measured in transverse sections of Al_2O_3–$ZrO_2(Y_2O_3)$ samples grown at different growth rates. XRD diagrams of α-Al_2O_3 and c-ZrO_2 are also given for comparison.

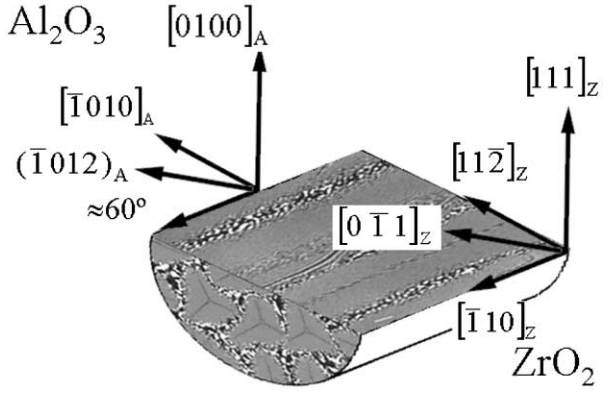

Fig. 4. Microstructure and phase crystallographic orientations of an Al_2O_3–$ZrO_2(Y_2O_3)$ eutectic sample grown at 300 mm/h. The longitudinal cross-section is the $(1\bar{2}10)$ Al_2O_3 crystallographic plane.

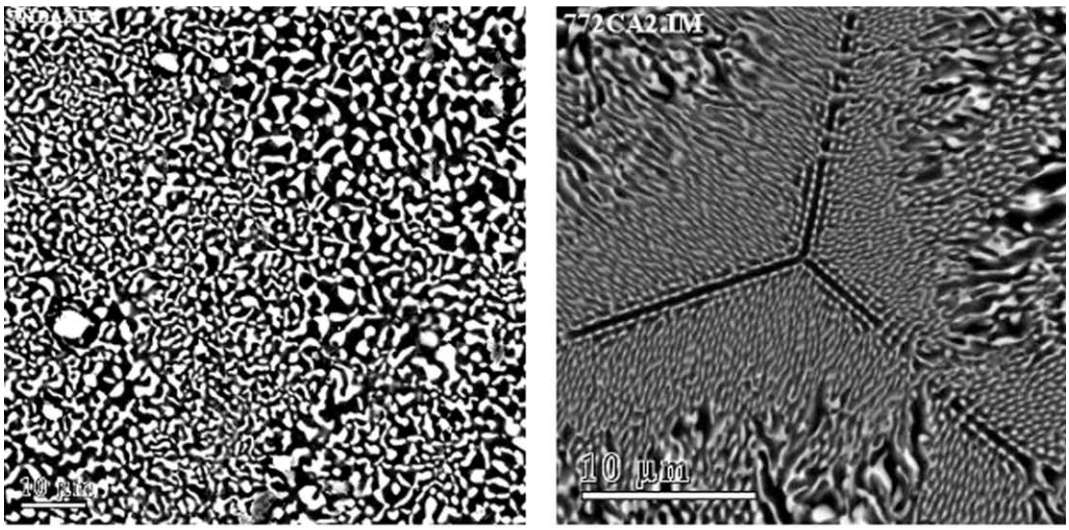

(a)

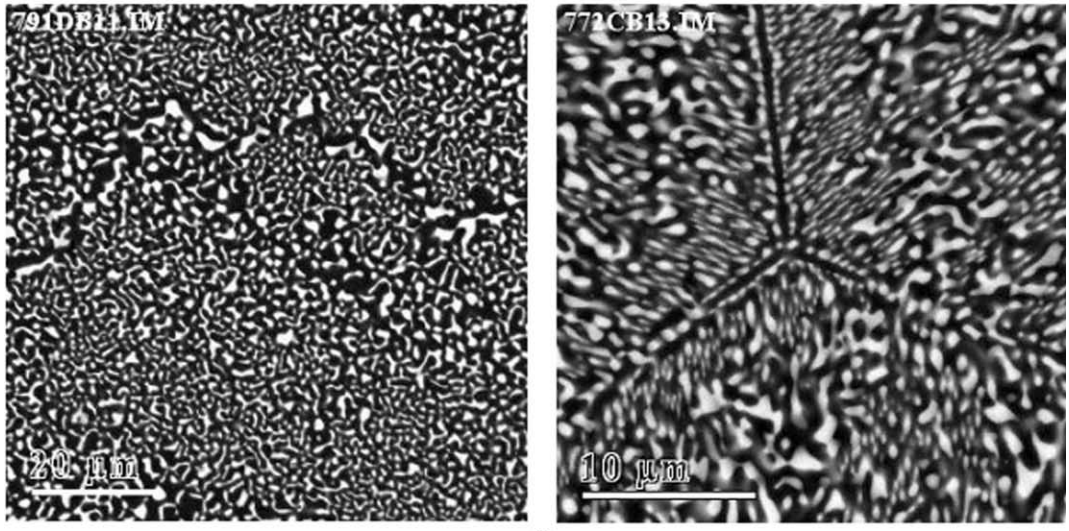

(b)

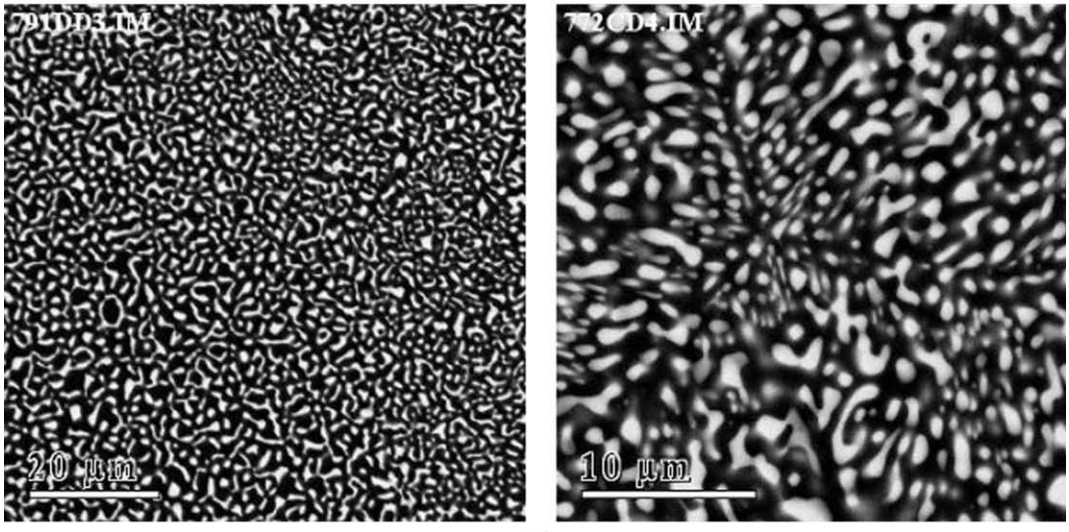

(c)

Fig. 5. SEM micrographs of transverse sections of Al_2O_3–$ZrO_2(Y_2O_3)$ eutectics grown at: left side, 10 mm/h and right side, 300 mm/h after heating in air at 1500 °C during: (a) 0, (b) 100 and (c) 340 h.

crystal 60° around the [0001] axis. In our model this reflects the presence some of the trigonal cells in antiparallel orientation (see Fig. 6).

From the width of the diffraction peaks in the alpha-scan patterns a misorientation of about 5° in the crystallographic directions attributed to some mosaic structure along the whole sample can be estimated. The orientation relationships between the different phases are:

$(\bar{1}012)_A//(01\bar{1}\bar{1})_Z$
$[\bar{2}\bar{2}01]_A//[1\bar{1}\bar{1}]_Z$
$[0100]_A//[111]_Z$

In the case of the eutectic samples with the interpenetrating microstructure grown at the lowest rate, the phase orientations clearly correspond to an interpenetrating bicrystal. In general the same growth habits described above are found. However, this general behavior breaks down in some cases where, although the bicrystal characteristic is preserved, the phases do not grow along a simple crystallographic direction. This result may be explained in light of the coupled growth dynamic. In this growth regime, the leading role of the phase with the highest entropy of fusion (the alumina phase) can be displaced to the benefit of the cooperative growth. This absence of faceted growth may introduce the observed variability in growth habit.

3.3. Thermal treatment

Samples from melt-grown rods containing either an interpenetrating or a colony microstructure were chosen for thermal stability studies. The thermal cycle was at 1500 °C in air for 24, 100 and 340 h (Fig. 5). The treated samples were polished to remove a few microns near the surface and studied by SEM. The microstructure was analyzed using Digital Micrograph software. The evolution of the microstructure is illustrated in Fig. 5. An evolution is observed inside the colonies, where the ordered fine fibrous structure of the zirconia phase is substituted by a coarser globular microstructure. The interpenetrating microstructure remains essentially unaltered by the thermal annealing.

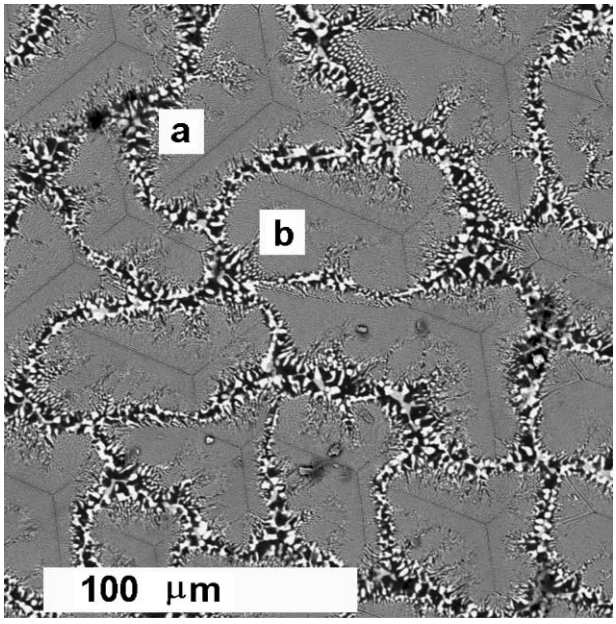

Fig. 6. SEM micrograph of a transverse section of Al_2O_3–$ZrO_2(Y_2O_3)$ eutectic grown at 300 mm/h showing colonies oriented antiparallel to each other. (See for example the ones labeled a and b.).

4. Conclusions

Al_2O_3–ZrO_2(9 mol% Y_2O_3) melt-growth composites were produced by the laser float zone method. The microstructure was studied as a function of the processing parameters and thermal gradient; growth rate and rod radius values for optimal crack free, homogeneous, interpenetrating microstructures were obtained. Thermal annealing experiments indicate that the interpenetrating coupled microstructure is stable during thermal treatments at high temperature. Crystallography studies determined the crystallographic growth habits with the sapphire phase usually growing along the *c*-axis and cubic zirconia along its [110] axis. Orientation relationships between the component phases were also obtained.

Acknowledgements

We gratefully acknowledge support from the Spanish Ministry of Science and Technology (CICYT MAT2000–1495 and MAT2000–1533-C03–02). N.R. Harlan also thanks the Ford Foundation (USA) for a fellowship. Dr M.C. Sanchez is acknowledged for his help in the XRD measurements.

References

1. Waku, Y., Nakagawa, N., Wakamoto, T., Ohtsubo, H., Shimizu, K. and Kohtoku, Y., *Nature (London)*, 1997, **389**, 49–52.
2. Stubican, V. S. and Bradt, R. C., *Ann. Rev. Mater. Sci.*, 1981, **11**, 267–297.
3. Sayir, A., Farmer, S. C., Dickerson, P. O. and Yun, H. M., *Mat. Res. Soc. Symp. Proc*, 1995, **365**, 21–27.
4. Pastor, J. Y., Poza, P., Llorca, J., Peña, J. I., Merino, R. I. and Orera, V. M., *Mater. Sci. Eng. A*, 2001, **308**, 241–249.
5. Schmid, F. and Viechnicki, D., *J. Mater. Sci.*, 1970, **5**, 470–473.
6. Echigoya, J., Takabayashi, Y., Suto, H. and Ishigame, M., *J. Mater. Sci. Lett.*, 1986, **5**, 150–152.
7. Courtright, E. L., Haggerty, J. S. and Sigalovsky, J., *Ceram. Eng. Sci. Proc*, 1993, **14**, 671–681.
8. Starostin, M.Yu., Gnesin, B. A. and Yalovets, T. N., *J. Cryst. Growth*, 1997, **171**, 119–124.

9. Lee, J. H., Yoshikawa, A., Kaiden, H., Lebbou, K., Fukuda, T., Yoon, D. H. and Waku, Y., *J. Cryst. Growth*, 2001, **231**, 179–185.
10. Larrea, A., de la Fuente, G. F., Merino, R. I. and Orera, V. M., *J. Eur. Ceram. Soc.*, 2002, **22**, 191–198.
11. Pardo, J. A., Merino, R. I., Orera, V. M., Peña, J. I., Gonzalez, C., Pastor, J. Y. and Llorca, J., *J. Am. Ceram. Soc.*, 2000, **83**, 2745–2752.
12. Borodin, V. A., Starostin, M.Yu. and Yalovets, T. N., *J. Cryst. Growth*, 1990, **104**, 148–153.
13. Yoshikawa, A., Hasegawa, K., Lee, J. H., Durbin, S. D., Epelbaum, B. M., Yoon, D. H., Fukuda, T. and Waku, Y., *J. Cryst. Growth*, 2000, **218**, 67–73.
14. Lakiza, S. M. and Lopato, L. M., *J. Am. Ceram. Soc.*, 1997, **80**, 893–902.
15. de la Fuente, G. F., Dıez, J. C., Angurel, L. A., Peña, J. I., Sotelo, A. and Navarro, R., *Adv. Mater.*, 1995, **7**, 853–856.
16. Nason, D. O., Yen, C. T. and Tiller, W. A., *J. Cryst. Growth*, 1990, **106**, 221–226.
17. Hunt, J.D. and Shu-Zu, Lu, In *Handbook of Crystal Growth*, Vol 2, ed. D.T.J. Hurle. Elsevier Science B.V., 1994, pp. 1113–1164.
18. Lee, Y. C. and Chen, J. C., *Optical Materials*, 1999, **12**, 83–91.
19. Brice, J. C., *J. Cryst. Growth*, 1977, **42**, 427–430.
20. Tong, L., *J. Cryst. Growth*, 2000, **217**, 281–286.
21. Bourban, S., Karapatis, N., Hofmann, H. and Kurz, W., *Acta Mater.*, 1997, **45**, 5069–5075.
22. Burden, M. H. and Hunt, J. D., *J. Cryst. Growth*, 1974, **22**, 328–330.
23. Tatarchenko, V. A., Yalovets, T. N., Satunkin, G. A., Zatulovsky, L. M., Egorov, L. P. and Kravetsky, D.Ya., *J. Cryst. Growth*, 1980, **50**, 335–340.